

# The effect of flaw on rock mechanical properties under the Brazilian test

Yu Zhou\*, Guang Zhang, Shunchuan Wu, Li Zhang

Key Laboratory of Ministry of Education for Efficient Mining and Safety of Metal Mine, University of Science and Technology Beijing,  
Beijing 100083, China

\*Corresponding author: westboy85@sina.com.cn

## Abstract

Tensile strength is one of the most significant parameters for rock. Rock-like materials were used to prefabricate Brazilian disc specimens containing a single flaw. Meanwhile, based on particle flow theory and the particle flow code 2 dimension (PFC2D) program, the effects of flaw length and dip angle on the specimens' mechanical properties under Brazilian test were investigated, and a formula for tensile strength of specimens containing a single flaw under the Brazilian test was constructed. The results are shown as follows. When the flaw length is consistent, the tensile strength of specimens decreases initially and then increases with an increase in the flaw dip angle. When the flaw dip angle is consistent, the tensile strength of specimens decreases gradually with an increase in the flaw length. With an increase in the flaw length, the effect of flaw on the failure mode of specimens becomes more pronounced, and the amount of acoustic emission decreases and the distribution range of fracture magnitude shrinks.

**Keywords:** Brazilian test; flaw; fracture mechanism; particle flow theory; tensile strength.

## 1. Introduction

Tensile strength is one of the most significant parameters for rock. At present, the Brazilian test is a general method to measure rock tensile strength, and it plays a major role in research fields such as rock mechanics theory, experiment and engineering application. The advantage of the Brazilian test is its ease of use, in that only an ordinary press machine is required to conduct the test.

The Brazilian test for rock strength measurement is over 40 years old. In 1971, Mellor & Hawkes (1971) investigated in depth the validity of the Brazilian test for rock strength measurement. Based on their research conclusions, the International Society for Rock Mechanics ISRM (1978) recommended the Brazilian test method as an indirect method to measure rock tensile strength in 1978. In recent years, scholars have carried out experimental and theoretical research of various rocks using the Brazilian test. Markides *et al.* (2010) used the complex function method to derive the analytical solution stress and displacement field of specimen under the Brazilian test. Through experimentation and simulation, Yu & Zhang (2009), Erarslan *et al.* (2012a) and Erarslan & Williams (2012b) investigated the stress state and failure process of specimens with different arc loading angles under the Brazilian test. Based on the analytic method established by Lekhnitskii (1968), Amadei *et al.* (1983) derived a generalized analytic formula of anisotropic disc material under the Brazilian test. Istvan *et al.* (1997), McLamore & Gray (1967), Chen *et al.* (1998) and Debecker & Vervoort (2009) investigated the relationship between beddings and tensile strength based on transverse isotropical rocks such as sandstone, slate and coal, respectively.

As one kind of widely developed geologic structure, flaws are significant factors that influence the strength, deformation and fracture mechanism in rock. The mechanical characteristics of rock containing flaws under uniaxial or triaxial compressive conditions have been widely researched (Wong & Einstein, 2009a; Wong & Einstein, 2009b; Yang *et al.*, 2008; Huang *et al.*, 2016). However, few reports have examined the mechanical characteristics of specimens containing a flaw from a meso mechanical viewpoint. Therefore, in this paper, rock-like materials were used to prefabricate Brazilian disc specimens containing a single flaw. Further, based on particle flow theory and PFC2D program, the effects of flaw length and dip angle on the specimens' mechanical properties under Brazilian test were investigated, and a tensile strength formula for specimens containing a single flaw under the Brazilian test was constructed.

## 2. Experimental study

### 2.1 Specimen preparation and test procedures

In the Brazilian test, cement, fine sand and water are mixed at a ratio of 4:2:1 to construct the specimens. The shape of specimens in the Brazilian test is cylinder, with a diameter of 50mm and height of 30mm. A single flaw with a width of 1.5mm, is precasted in the center of the specimen. The length L of the flaw is set to 0 mm, 8mm and 24mm, and the dip angle (the angle between the flaw and the loading direction)  $\alpha$  of the flaw is set to 0°, 15°, 30°, 45°, 60°, 75° and 90°.

A WEP-600 universal testing machine is used as the loading machine. The test loading rate is set to 0.3MPa~0.5MPa per second. When an obvious fracture sound is generated or the data value of loading sensor decreases suddenly, the test is stopped.

2.2 Test results

2.2.1 Tensile strength

The average value of tensile strength for an intact specimen is 3.80MPa. As shown in Table 1, when a flaw exists and its length is constant, the tensile strength  $\sigma_t$  of specimens

decreases initially and then increases, with an increase in the flaw dip angle. When the flaw dip angle  $\alpha$  equals  $0^\circ$  or  $90^\circ$ , the specimens possess relatively high tensile strength. When the flaw dip angle  $\alpha$  equals  $45^\circ$ , the tensile strength of specimens reaches its minimum value. For example, when flaw length  $L$  equals 8mm and 24mm, the tensile strength of specimens is 2.17MPa and 0.94MPa, respectively. Moreover, under the condition of the same flaw dip angle, the tensile strength of specimens decreases gradually with an increase in the flaw length.

**Table 1.** Tensile strength of specimens with different flaw conditions.

Flaw dip angle $\alpha$ ( $^\circ$ )	Tensile strength $\sigma_t$ / MPa	
	Flaw length $L=8\text{mm}$	Flaw length $L=24\text{mm}$
0	2.93	1.59
15	-	1.36
30	2.52	1.13
45	2.17	0.94
60	2.33	1.33
75	-	1.35
90	2.74	1.28

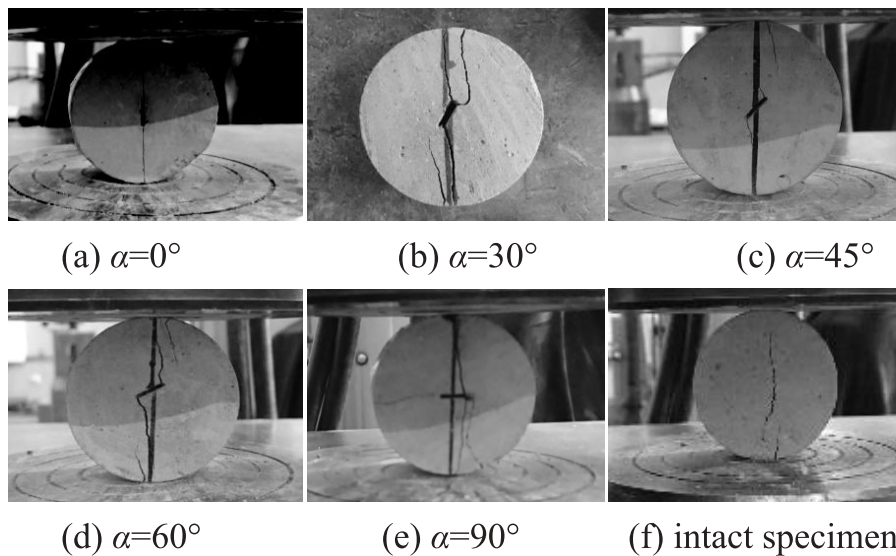
2.2.2 Fracture distribution

Figure 1 and Figure 2 show the fracture distribution of specimens after the Brazilian test when the flaw length is 8mm and 24mm, respectively.

When the specimen is intact, the fracture mainly propagates along the loading direction in specimen. Because of the end effect, some fractures present an angle towards the loading direction and originate at the loading part of specimen.

As shown in Figure 1 and Figure 2, when the specimen contains a single flaw, the fracture distribution state is influenced by the flaw condition in different degrees under the Brazilian test.

When the flaw dip angle  $\alpha=0^\circ$ , the two types of specimen containing different flaw lengths have similar distributions of fractures, which primarily generate along the loading direction between the loading ends and the flaw tips of the specimen.



**Fig. 1.** Fracture distribution of a specimen with a flaw length of 8 mm.

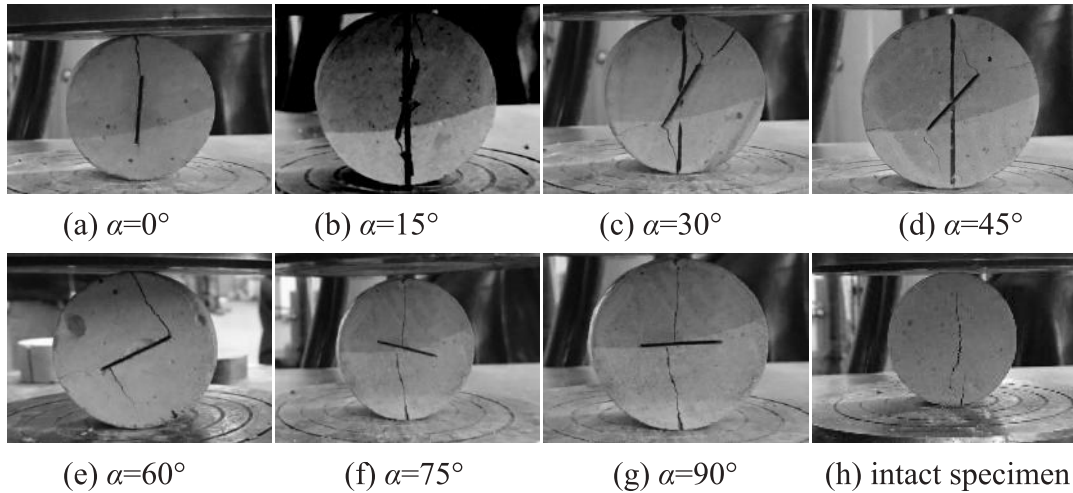


**Fig. 2.** Fracture distribution of a specimen with a flaw length of 24 mm.

With a flaw length of 8mm, the fracture characteristic of the specimen is as follows. When the flaw dip angle is 30°, 45° and 60°, two fractures generate between the loading ends and flaw tips of the specimen and intersect at the flaw tips. The width between these fractures is narrow. When the flaw dip angle is 90°, fractures mainly generate between the loading ends and the flaw tips.

With a flaw length of 24mm, the fracture characteristic of the specimen is as follows. When the flaw dip angle is 15°, 30°, 45° and 60°, two fractures generate between the loading ends and the flaw tips. With an increase in the flaw dip angle, the angle between the fractures at the flaw tips also increases. One fracture generates between the loading ends and the flaw tips, and the other generates mainly along the flaw trend direction. When the flaw dip angle is 75° and 90°, fractures generate mainly between the centre part of the flaw and the loading end.

### 3. Numerical simulation

#### 3.1 Meso mechanical parameter determination

Based upon the discrete element method, Cundall & Strack (1979) established particle flow theory by introducing the idea of molecular dynamics. This theory emphasizes the explanation of the damage and fracture mechanism of material from a meso mechanical viewpoint, analyzing the process of large deformation from the linear elastic stage to rupture failure and considering the process of crack formation, propagation and coalescence intuitively. Hence,

it is very suitable for investigating the mechanical and engineering characteristics of rock. Based on the particle flow theory, the particle flow code uses particle elements to construct a calculative model, and does not need to define the macroscopic constitutive relation of material in advance. It only needs to set the meso mechanical parameters between particles, and the intricate nonlinear stress-strain relationship can be determined automatically with the stress condition. Simultaneously, bonds between particles that can be broken are affected by external action, which results in the mutual separation of particles, for implementing a numerical simulation of crack generation and propagation in the material.

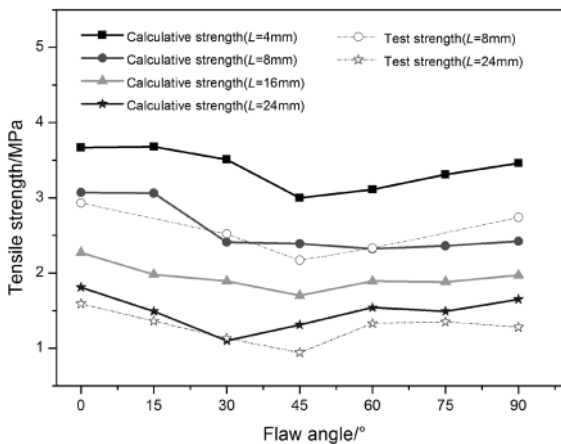
In this paper, based on particle flow theory and the PFC2D program, the numerical models are constructed with the same size as the specimens. Based on the experimental data of the intact specimen, the meso mechanical parameters shown in Table 2 are obtained by repeated debugging. To ensure the quasi-static loading state, the loading strain rate (1.0) is set to be sufficiently small in the simulation, and the calculative termination condition is established when the residual strength reaches 40% of the peak strength. The calculative tensile strength of the intact specimen is 3.83MPa, based on the meso mechanical parameters of table 2. This calculative tensile strength is consistent with the test result. Therefore, the meso mechanical parameters are reasonable and can be used for the remaining simulations.

**Table 2.** Calculated meso/mechanical parameters.

Minimum particle radius, $R_{\min}/\text{mm}$	Particle radius ratio, $R_{\text{rat}}$	Bulk density, $\rho/(\text{kg}\cdot\text{m}^{-3})$	Friction coefficient, $\mu$	Contact elastic modulus, $E_c/\text{GPa}$	Stiffness ratio of normal and shear contact, $k_n/k_s$	
0.25	1.75	2500	0.5	15.0	3.1	
Radius coefficient of parallel bond, $\lambda$	Elastic modulus of parallel bond, $\bar{E}_c$	Stiffness ratio of normal and shear parallel bond, $\bar{k}_n/\bar{k}_s$	Normal strength of parallel bond		Shear strength of parallel bond	
			Average value, $\sigma_{n\text{-mean}}/\text{MPa}$	Standard deviation, $\sigma_{n\text{-dev}}/\text{MPa}$	Average value, $\tau_{s\text{-mean}}/\text{MPa}$	Standard deviation, $\tau_{s\text{-dev}}/\text{MPa}$
1.0	15.0	3.1	15.8	1.58	15.8	1.58

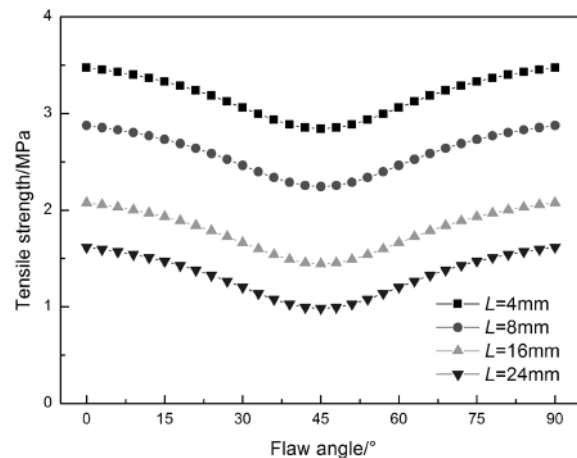
### 3.2 Effect of flaw on tensile strength

Figure 3 shows the numerical and experimental results of specimens with different flaw conditions under the Brazilian test. It is clear that when the flaw length  $L$  equals 8mm and 24mm, the calculation is approximately the same as the experimental value, and the variation law is similar. This again indicates that the calculative meso mechanical parameters shown in Table 2 can represent the mechanical properties of test sample very well. A similar result was obtained when the flaw dip angle was constant: the calculative tensile strength decreased gradually with an increase in the flaw length. When the flaw length is constant, the calculative tensile strength decreases initially and then increases with an increase in the flaw dip angle. With this flaw condition, the tensile strength reaches a minimum value when the flaw dip angle is approximately  $45^\circ$ , and it reaches a relatively high value with the dip angle of  $0^\circ$  or  $90^\circ$ . This calculative results show that when the flaw length  $L$  equals 4mm, 8mm, 16mm and 24mm, the specimens reach the minimum value of 3.00MPa, 2.32MPa, 1.70MPa and 1.10MPa, with a flaw dip angle of  $45^\circ$ ,  $60^\circ$ ,  $45^\circ$  and  $30^\circ$ , respectively.

**Fig. 3.** Tensile strength with different flaw lengths.

The effect of the flaw length  $L$  and dip angle  $\alpha$  on the strength of Brazilian test specimens containing a single flaw was investigated. Based on the simulation results, the relational expression among the flaw length, dip angle and strength is shown as Equation (1). As shown in Figure 4, the strength analytical solution of Brazilian test specimens with different flaw condition is calculated by Equation (1), and its variation law is consistent with the experimental and simulation results. In Equation (1),  $L$ ,  $\alpha$  and  $D$  are the flaw length, flaw dip angle and specimen diameter, respectively.  $A$  and  $\alpha$  are the curve shape parameter, respectively. In this paper,  $A$  is 60, and  $\alpha$  is 45.

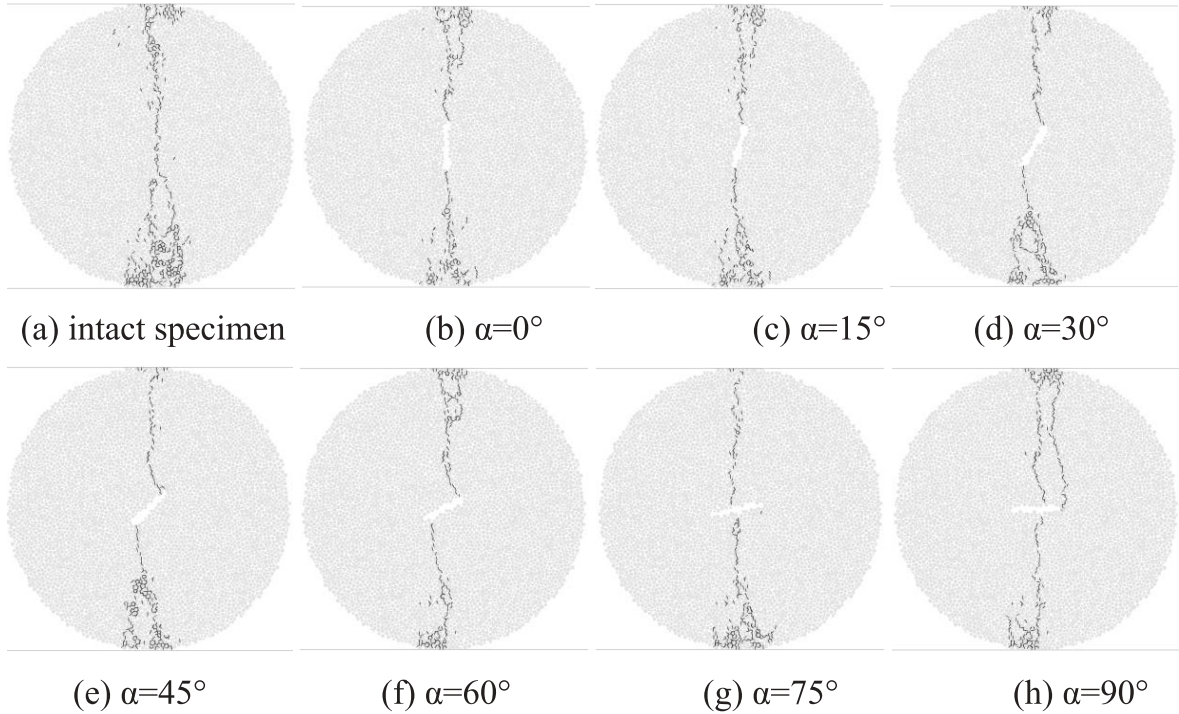
$$\sigma_t = \sigma_{t0} \cdot \left[ 0.309 + 0.855 \exp\left(-\frac{L}{0.290D}\right) \right] - \frac{2A}{\pi} * \frac{w}{4(\alpha - 45)^2 + w^2} \quad (1)$$

**Fig. 4.** Analytical solution of tensile strength.

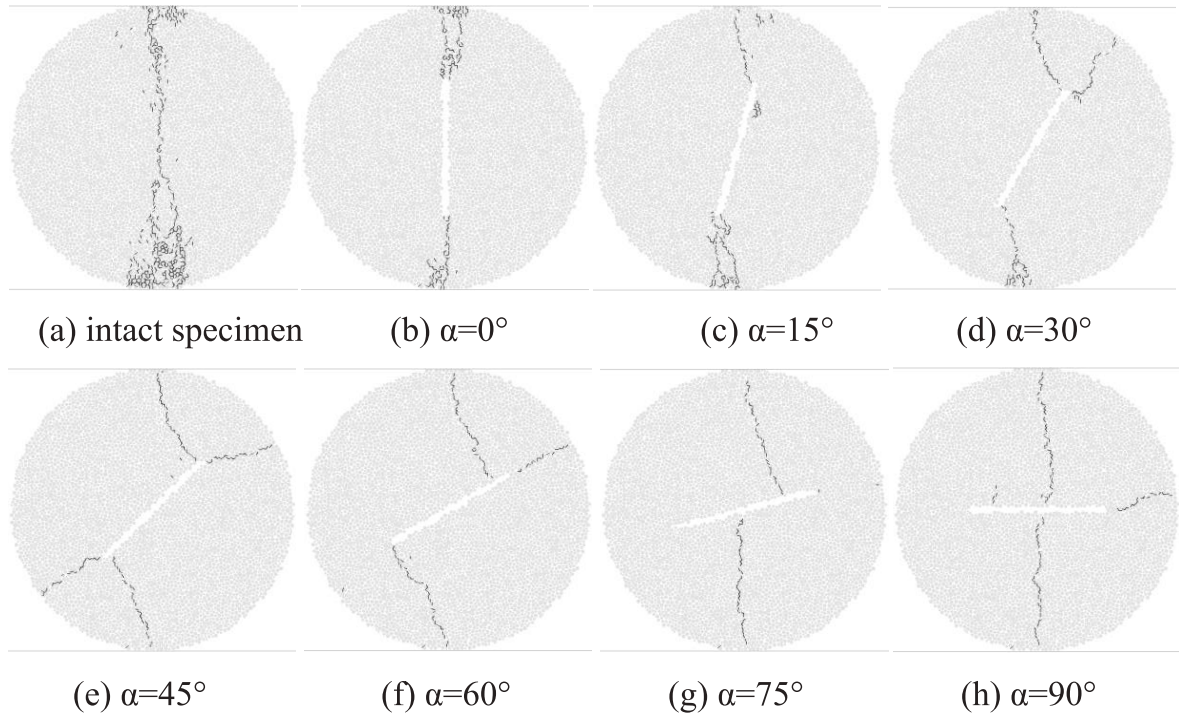
3.3 Effect of flaw on micro-crack distribution

Figure 5 and Figure 6 show the micro-crack distribution when the flaw length of specimens is equal to 8mm and 24mm, respectively. The short red and blue short lines represent a

tensile and shear micro-crack, respectively. It appears that the tensile micro-crack dominates in specimen failure under this two-flaw condition.



**Fig. 5.** Micro-crack distribution (Flaw length  $L=8$  mm).



**Fig. 6.** Micro-crack distribution (Flaw length  $L=24$  mm).

When the flaw length  $L$  is equal to 0mm or 8mm, the micro-cracks located in the loading part of specimen are intensive and consist of some shear micro-cracks. When the flaw length  $L$  is equal to 24mm, micro-cracks that are located in the loading part of specimen decrease with an increase in the flaw dip angle. The shape of the fracture formed by micro-cracks becomes narrower.

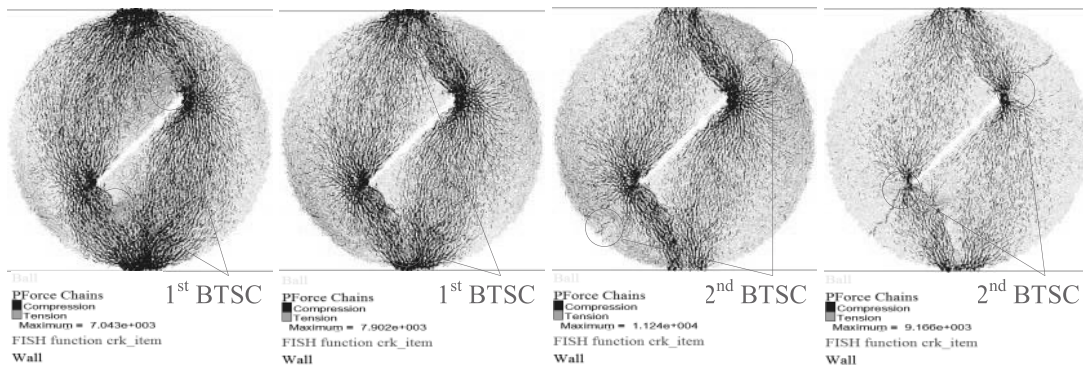
When the flaw length  $L$  equals 8mm, micro-cracks mainly form between the loading ends and flaw tips with a flaw dip angle of  $0^\circ$ ,  $15^\circ$ ,  $30^\circ$ ,  $45^\circ$  and  $60^\circ$ . With a flaw dip angle of  $75^\circ$ , the micro-cracks mainly form between the central part of the flaw and the loading end. With a flaw dip angle of  $90^\circ$ , micro-cracks mainly form between the central part of flaw, the flaw and the loading end.

When the flaw length  $L$  equals 24mm, micro-cracks mainly form between the loading ends and flaw tips with a flaw dip angle of  $0^\circ$  and  $15^\circ$ . With a flaw dip angle of  $30^\circ$ ,  $45^\circ$  and  $60^\circ$ , a portion of the micro-cracks form between loading ends and flaw tips: the others form along the direction of flaw trend. With a flaw dip angle of  $75^\circ$  and  $90^\circ$ , micro-cracks mainly generate between the central part of the flaw and the

particles occurring twice during the loading process (see in Figure 7). The first BTSC occurred at the flaw tips initially, and gradually developed towards the closest loading boundary. The second BTSC initiated at the specimen boundary and trended towards the flaw tips. When the BTSC exceeds the bond tensile strength between particles, the tensile cracks form, resulting in two fractures at the flaw tips.

### 3.4 Effect of flaw on acoustic emission characteristics

Influenced by the action of external force, internal force or temperature, some of the cracks generated and extended during the rock failure process, accompanied by the phenomenon of strain energy release and transient elastic wave generation. This phenomenon is called acoustic emission (AE). Based on particle flow theory and PFC2D program, Hazzard & Young (2000; 2002; 2004) established the AE simulation method for rock material on the meso scale. In this paper, four typical specimens (intact sample; sample with  $L=8\text{mm}$  and  $\alpha=0^\circ$ ; sample with  $L=24\text{mm}$  and  $\alpha=45^\circ$ ; sample with  $L=24\text{mm}$  and  $\alpha=90^\circ$ ), were selected to investigate the evolution rule of micro-cracks of Brazilian test specimens containing different flaws by using the AE simulation method. In the simulation



(a) Initiation of 1<sup>st</sup> BTSC (b) End of 1<sup>st</sup> BTSC (c) Initiation of 2<sup>nd</sup> BTSC (d) End of 2<sup>nd</sup> BTSC

**Fig. 7.** The mechanism of the generation of two fractures at the flaw tips.

loading end. Moreover, portions of the micro-cracks form along the direction of the flaw trend with a flaw dip angle of  $90^\circ$ .

In summary, with an increase in the flaw length, the effect of flaw on the failure mode of specimen is more pronounced. When the flaw dip angle is constant, with an increase in the flaw length, the number of micro-cracks decreases gradually, and the fracture width formed by micro-cracks increases. Under different flaw conditions, the above calculative fracture distribution is consistent with the experimental results, which indicates that the simulation is reliable.

As an example, two fractures at the flaw tip formed in the specimen with a length of 24mm and dip angle of  $45^\circ$  due to the bond tensile stress concentration (BTSC) between

process, every circle represents a single AE event, and its size represents the AE magnitude.

Figures 8, 9, 10 and 11 show the AE event distribution under different flaw conditions. Based on these results, the micro-crack evolution rule of Brazilian test specimens containing different flaws was analysed as follows. When the specimen is intact, AE events initiated at the loading boundary, and then extended towards the centre of the specimen. When the flaw length  $L$  equalled 8mm and the dip angle  $\alpha$  equalled  $0^\circ$ , AE events initiated at the flaw tips, and then extended towards the loading boundary. When the flaw length  $L$  equalled 24mm and dip angle  $\alpha$  equalled  $45^\circ$ , AE event generation could be divided into two stages. In the first stage, AE events generated from the flaw tips to

the loading end. In the second stage, AE events generated from the specimen boundary to the flaw tips. When the flaw length  $L$  equalled 24mm and the dip angle  $\alpha$  equalled  $90^\circ$ , AE event generation could also be divided into two stages. In

the first stage, AE events generated from flaw centre to the loading end. In the second stage, AE events generated from the specimen boundary to the flaw tips.

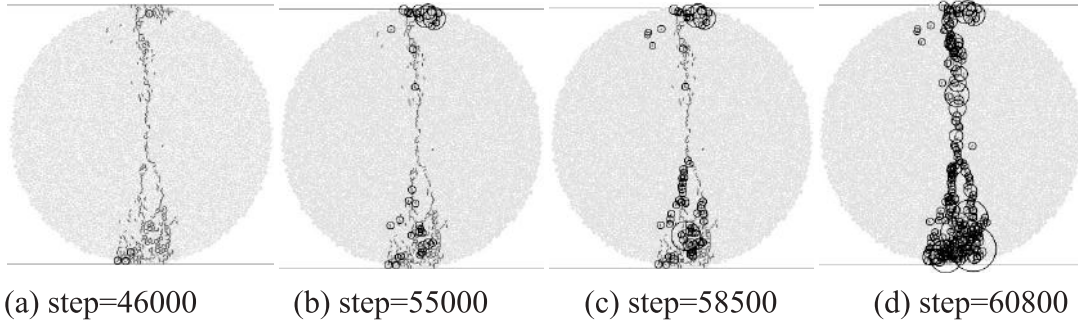


**Fig. 8.** AE event distribution of intact specimen.

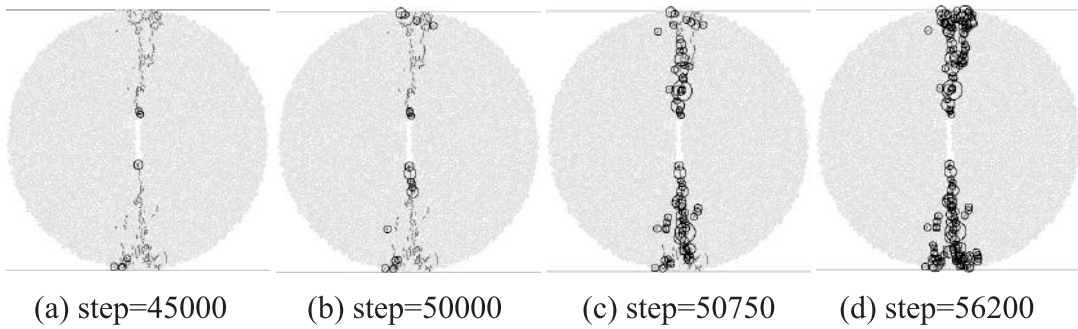


**Fig. 9.** AE event distribution of specimen with flaw length of 8 mm and dip angle of  $0^\circ$

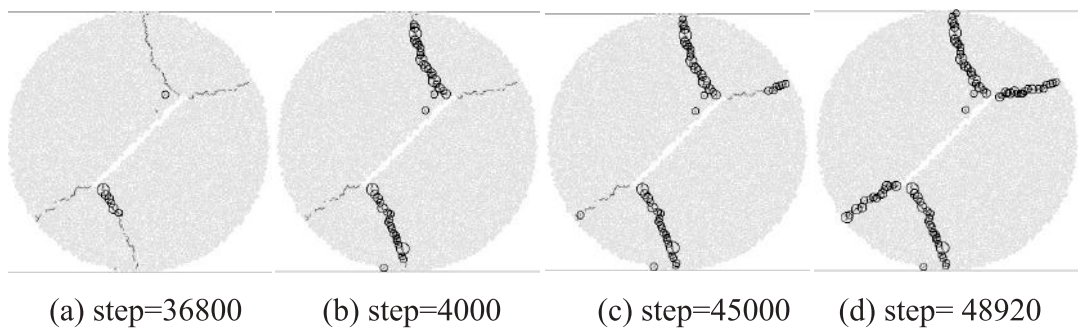


**Fig. 10.** AE event distribution of specimen with flaw length of 24 mm and dip angle of  $45^\circ$ .

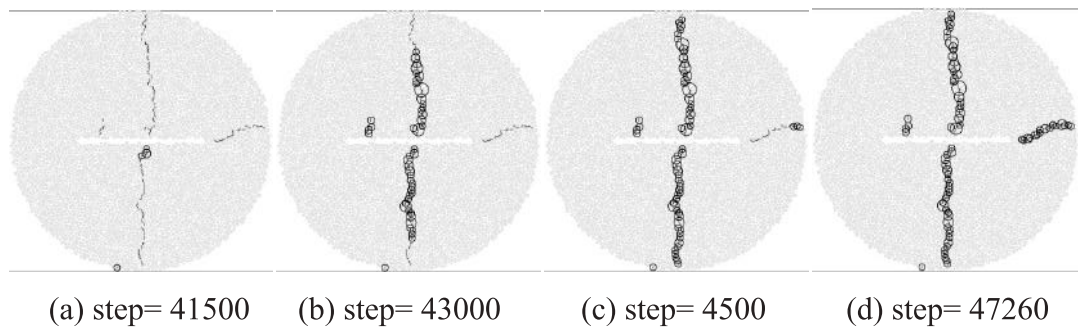


**Fig. 11.** AE event distribution of specimens with flaw length of 24 mm and dip angle of  $90^\circ$ .

Figure 12 shows the relationship between the AE count and the fracture magnitude. With respect to the relationship between AE count and fracture magnitude, in intact specimens, the number of AE event was 230, the maximum and minimum values of AE fracture magnitude were -4.6799 and -6.1246, and the mean value and standard deviation of AE fracture magnitude were -5.4023 and 1.0216, respectively.

When the flaw length  $L$  equals 8mm and the dip angle  $\alpha$  equals  $0^\circ$ , there are 147 AE events. The maximum and minimum values of AE fracture magnitude are -5.1092 and -6.2182, and the mean value and standard deviation of AE fracture magnitude are -5.6637 and 0.7842, respectively.

When the flaw length  $L$  equals 24mm and the dip angle  $\alpha$  equals  $45^\circ$ , there are 81 AE events. The maximum and minimum values of AE fracture magnitude are -5.2474 and

-5.9976, and the mean value and standard deviation of AE fracture magnitude are -5.6625 and 0.8305, respectively.

When the flaw length  $L$  equals 24mm and the dip angle  $\alpha$  equals  $90^\circ$ , there are 80 AE events. The maximum and minimum value of AE fracture magnitude are -5.2124 and -5.8131, and the mean value and standard deviation of AE fracture magnitude are -5.5127 and 0.4248, respectively.

As shown in Figure 12, some AE characteristics of Brazilian test specimens containing a single flaw are identified as follows. When the specimen is intact, the AE count is larger than that containing a single flaw and the AE fracture magnitude is larger. With an increase in the flaw length, the AE count decreases, and the range of AE fracture magnitude shrinks. However, the relationship between the AE count and fracture magnitude is essentially normally distributed.

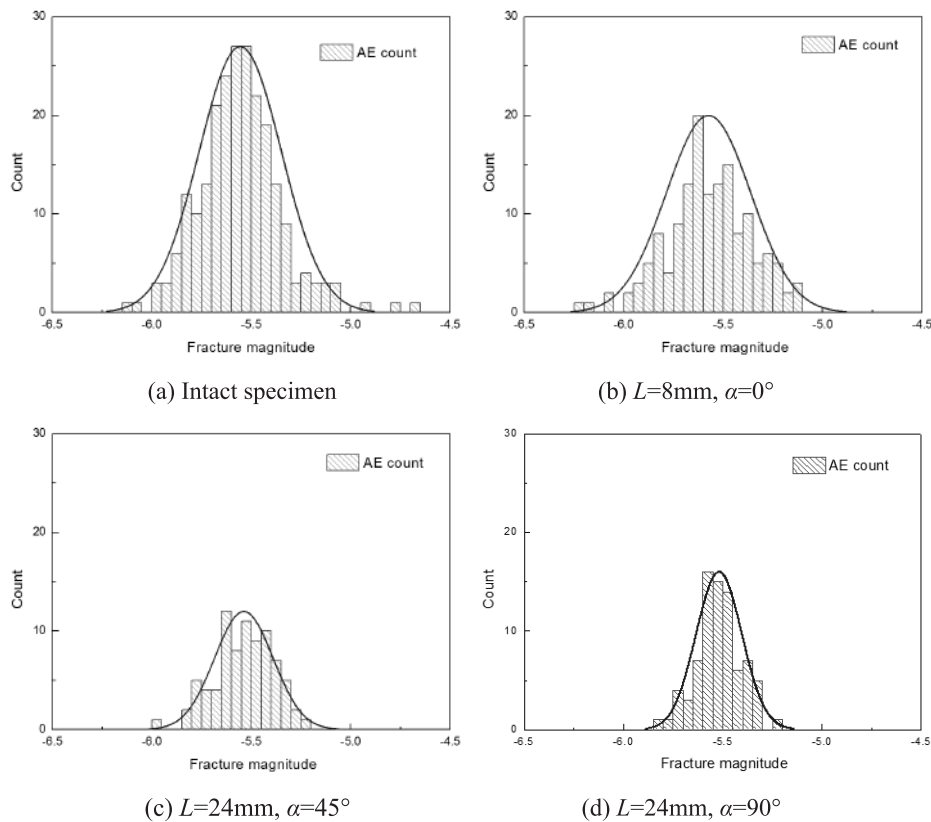


**Fig. 12.** Relationship between AE counts and fracture magnitude.

#### 4. Conclusion

The effect of flaw length and dip angle on specimen's mechanical properties in the Brazilian test was investigated in this paper. The experimental and numerical analyses show the following: (1) When the flaw length is consistent, the tensile strength of the specimens decreases initially and then increases with an increase in the flaw dip angle. (2) When the flaw dip angle is consistent, the tensile strength of the specimens decreases gradually with an increase in the flaw

length. (3) With an increase in the flaw length, the effect of the flaw on the failure mode of specimens becomes more remarkable. (4) With an increase in the flaw length, the amount of acoustic emission decreases.

#### 5. Acknowledgments

This work is financially supported by the National Natural Science Foundation of China (No. 51504016) and Fundamental Research Funds for the Central Universities (No. FRF-BD-17-007A).

## References

- Amadei, B., Rogers, J. D. & Goodman, R. E. (1983).** Elastic constants and tensile strength of the anisotropic rocks. Proceedings of the Fifth Congress of International Society of Rock Mechanics, Melbourne, Australia.
- Chen, C. S., Pan, E. & Amadei, B. (1998).** Determination of deformability and tensile strength of anisotropic rock using Brazilian tests. *International Journal of Rock Mechanics and Mining Sciences*, **35**(1): 43-61.
- Cundall, P. A. & Strack, O. D. L. (1979).** A discrete numerical model for granular assemblies. *Geotechnique*, **29**(1): 47-65.
- Debecker, B. & Vervoort, A. (2009).** Experimental observation of fracture patterns in layered slate. *International Journal of Fracture*, **159**(1): 51-62.
- Erarslan, N., Liang, Z. Z. & Williams, D. J. (2012a).** Experimental and numerical studies on determination of indirect tensile strength of rocks. *Rock Mechanics and Rock Engineering*, **45**(5): 739-751.
- Erarslan, N. & Williams, D. J. (2012b).** Experimental, numerical and analytical studies on tensile strength of rocks. *International Journal of Rock Mechanics and Mining Sciences*, **49**(1): 21-30.
- Hazzard, J. F. & Young, R. P. (2000).** Simulating acoustic emissions in bonded-particle models of rock. *International Journal of Rock Mechanics and Mining Sciences*, **37**(5): 867-872.
- Hazzard, J. F. & Young, R. P. (2002).** Moment tensors and micromechanical models. *Tectonophysics*, **356**(1-3): 181-197.
- Hazzard, J. F. & Young, R. P. (2004).** Dynamic modelling of induced seismicity. *International Journal of Rock Mechanics and Mining Sciences*, **41**(8): 1365-1376.
- Huang, D., Gu, D. M., Yang, C., Huang, R. Q. & Fu, G. Y. (2016).** Investigation on mechanical behaviors of sandstone with two preexisting flaws under triaxial compression. *Rock Mechanics and Rock Engineering*, **49**(2): 375-399.
- Istvan, J. A., Evans, L. J., Weber, J. H. & Devine, C. (1997).** Rock mechanics for gas storage in bedded salt caverns. *International Journal of Rock Mechanics and Mining Sciences*, **34**(3-4): 142.e1-142.e12.
- ISRM. (1978).** Suggested methods for determining tensile strength of rock materials. *Journal of Rock Mechanics and Mining Sciences and Geomechanics Abstract*, **15**(3): 99-103.
- Lekhnitskii, S. G. (1968).** Anisotropic plates. Gordon and Breach Scientific Publications, New York, 369-370.
- Markides, C. F., Pazis, D. & Kourkoulis, S. (2010).** Closed full-field solutions for stresses and displacements in the Brazilian disk under distributed radial load. *International Journal of Rock Mechanics and Mining Sciences*, **47**(2): 227-237.
- McLamore, R. & Gray, K. E. (1967).** The mechanical behavior of the anisotropic sedimentary rocks. *Journal of Engineering for Industry*, **89**(1): 62-73.
- Mellor, M. & Hawkes, I. (1971).** Measurement of tensile strength by diametral compression. *Engineering Geology*, **5**(2): 173-225.
- Wong, L. N. Y. & Einstein, H. H. (2009a).** Crack Coalescence in Molded Gypsum and Carrara Marble: Part 1 – Macroscopic Observations and Interpretation. *Rock Mechanics and Rock Engineering*, **42**(3): 475-511.
- Wong, L. N. Y. & Einstein, H. H. (2009b).** Crack Coalescence in Molded Gypsum and Carrara Marble: Part 2 – Microscopic Observations and Interpretation. *Rock Mechanics and Rock Engineering*, **42**(3): 513-545.
- Yang, S. Q., Jiang, Y. Z., Xu, W. Y. & Chen, X. Q. (2008).** Experimental investigation on strength and failure behavior of pre-cracked marble under conventional triaxial compression. *International Journal of Solids and Structures*, **45**(17): 4796-4819.
- Yu, Y. & Zhang, J. (2009).** A modified Brazilian disk tension test. *International Journal of Rock Mechanics and Mining Sciences*, **46**(2): 421-425.

Submitted: 23/11/2016

Revised : 14/02/2017

Accepted : 18/03/2017

## تأثير التصدع على الخواص الميكانيكية الخاضعة للاختبار البرازيلي

يوزو\*، جوانج زانج، شونشوان وو، لي زانج

المختبر الرئيسي لوزارة التعليم لكفاءة المناجم والأمان لمناجم المعادن، جامعة بكين للعلوم والتكنولوجيا، بكين 100083، الصين، بكين

\*westboy85@sina.com.cn

### الملخص

تعتبر قوة تحمل الشد أحد أهم معلمات الصخور. تم استخدام مواد مشابهة للصخور لتصنيع عينات من القرص البرازيلي تحتوي على صدع واحد. اعتماداً على نظرية تدفق الجزيئات وبرنامج مقياس تدفق الجزيئات (PFC2D) تم بحث تأثير طول الصدع وزاوية التصدع على الخواص الميكانيكية للعينة تحت الاختبار البرازيلي. وتوضح النتائج في التالي: عندما يكون طول الصدع متناغم، تنخفض في البداية قوة تحمل الشد ثم تزداد مع زيادة زاوية التصدع. عندما تكون زاوية التصدع متناغمة، تنخفض قوة تحمل الشد بالتدرج مع زيادة طول الصدع. مع زيادة طول الصدع يصبح تأثير الصدع على نوعية الفشل للعينة أكثر ظهوراً وتتناقص كمية الانبعاثات الصوتية وينكمش مجال التوزيع لكمية الشروخ.